Construction and Building Materials 502 (2025) 144440

Contents lists available at ScienceDirect

Construction and Building Materials

journal homepage: www.elsevier.com/locate/conbuildmat

Enhanced thermoelectric and mechanical properties in cementitious composites via polymer-assisted dispersion of multiwalled carbon nanotubes

Jae In Lee [a,1], Suk Hoon Lim [b,1], Inyoung Lee [c], Kyungwho Choi [d], Jung Sang Cho [e], Sejin Choi [a,*], Chungyeon Cho [b,f,**]

[a] Department of Architectural Engineering, Wonkwang University, Iksan 54538, Republic of Korea
[b] Department of Carbon Convergence Engineering, College of Engineering, Wonkwang University, Iksan 54538, Republic of Korea
[c] Department of Chemical Engineering, College of Engineering, Wonkwang University, Iksan 54538, Republic of Korea
[d] School of Mechanical Engineering, Sungkyunkwan University, Suwon 16419, Republic of Korea
[e] Department of Engineering Chemistry, Chungbuk National University, Chungbuk 361-763, Republic of Korea
[f] Department of Biomedical Materials Science, Jeonbuk Advanced Bio-convergence Academy, Wonkwang University, Iksan, Jeonbuk 54538, Republic of Korea

ARTICLE INFO

Keywords:
Thermoelectric
Cementitious composite
PEDOT:PSS
Carbon nanotubes
Mechanical strength

ABSTRACT

The development of multifunctional construction materials capable of both structural support and direct energy harvesting from environmental temperature gradients represents a significant step toward sustainable, self-powered infrastructure. In this study, we present a novel and scalable strategy for fabricating thermoelectric (TE) cement composites by employing an aqueous suspension of poly(3,4-ethylenedioxythiophene) polystyrene sulfonate (PEDOT:PSS) as a multifunctional dispersant for multi-walled carbon nanotubes (MWNT). This hybrid network enables the cement matrix to convert waste heat into electrical energy while maintaining mechanical integrity and thermal stability, thereby allowing structural elements to function simultaneously as energy-harvesting modules. The synergy between the MWNT network and the PEDOT:PSS phase enables simultaneous improvement of electrical conductivity, Seebeck coefficient (S), and mechanical strength while maintaining thermal stability. Varying MWNT content revealed a percolation threshold near 0.5 wt%, producing a 4.3-fold conductivity increase and stable conductive pathways at higher loadings. The S displayed non-monotonic behavior due to the interplay between enhanced carrier transport and increased carrier concentration. Thermal conductivity rose moderately with MWNT addition via phonon transport along interconnected nanotube pathways, but remained low enough to sustain TE efficiency. The optimized composite achieved a power factor of 1.33×10^{-5} μW/m•K^2 and a ZT of 3.53×10^{-9} at room temperature. At 0.5 wt% MWNT, a peak 28-day compressive strength of 33.1 MPa (19.5 % higher than plain cement) was obtained. These findings highlight the potential of MWNT/PEDOT:PSS-modified cement as a robust platform for integrating structural performance with thermoelectric energy harvesting in infrastructure applications.

1. Introduction

The rapid pace of global industrialization and urbanization has precipitated an unprecedented surge in energy consumption, which is largely met by the combustion of fossil fuels [1]. This reliance has led to a critical escalation in greenhouse gas emissions, driving climate change and environmental degradation. A significant portion of this consumed energy, estimated to be over two-thirds, is dissipated into the environment as low-grade waste heat from industrial processes, vehicles, and even building envelopes [2]. In response to this challenge, the scientific community is intensely focused on developing sustainable and eco-friendly energy conversion technologies capable of harvesting this

* Corresponding author.
** Corresponding author at: Department of Biomedical Materials Science, Jeonbuk Advanced Bio-convergence Academy, Wonkwang University, Iksan, Jeonbuk 54538, Republic of Korea.
E-mail addresses: csj2378@wku.ac.kr (S. Choi), cncho37@wku.ac.kr (C. Cho).
[1] Equal contribution: Jae In Lee and Seok Hoon Lim contributed equally to this study.

https://doi.org/10.1016/j.conbuildmat.2025.144440
Received 20 July 2025; Received in revised form 26 October 2025; Accepted 5 November 2025
Available online 10 November 2025

abundant but diffuse waste heat. Among the various approaches, thermoelectric (TE) technology, which enables the direct, solid-state conversion of thermal gradients into useful electrical energy via the Seebeck effect, has emerged as a particularly promising solution for decentralized power generation and low-grade heat recovery [3,4]. The efficiency of a TE material is quantified by a dimensionless figure of merit, ZT. The ZT value is defined by the equation; $ZT = \sigma \bullet S^2 \bullet T/k$, where S is the Seebeck coefficient, σ is the electrical conductivity, k is the thermal conductivity, and T is the absolute temperature. To maximize ZT, a material must paradoxically possess a high σ, a large S and a low k. These properties are intrinsically coupled and often conflicting; for instance, materials with high σ typically also have high k due to the contribution of charge carriers to heat transport, as described by the Wiedemann-Franz law [5,6].

For decades, the field has been dominated by conventional inorganic semiconductors such as bismuth telluride (Bi_2Te_3), lead telluride (PbTe), and their alloys, which exhibit excellent ZT values near room temperature [7–9]. However, their widespread deployment is severely constrained by significant drawbacks, including the toxicity of their constituent elements (e.g., lead), mechanical brittleness, high processing costs, and the relative scarcity of elements such as tellurium [10,11]. These limitations have spurred research into alternative material systems. Organic TE materials, particularly conductive polymers, offer a compelling alternative [12–14]. Polymers such as poly(3, 4-ethylenedioxythiophene) doped with polystyrene sulfonate (PEDOT:PSS) are attractive due to their intrinsic advantages, including low cost, abundance of constituent elements, solution processability, inherent mechanical flexibility, and exceptionally low k [15,16]. While the power factor ($PF = \sigma \bullet S^2$) of pristine PEDOT:PSS is modest, it can be significantly enhanced through the creation of nanocomposites [17,18]. Incorporating high-aspect-ratio carbon nanomaterials, such as carbon nanotubes (CNT), into the polymer matrix has been shown to synergistically improve both σ and S by creating efficient charge percolation networks and introducing energy filtering effects at the polymer-nanotube interfaces [19–23].

Parallel to the development of flexible TE devices, a transformative approach has emerged that seeks to integrate TE functionality directly into the built environment [24–26]. Cement, the most widely used construction material on the planet, presents an ideal platform for embedding large-scale energy-harvesting capabilities. Its ubiquity, proven mechanical strength, and inherent low k (typically around 1.0–2.0 W/m·K) make it a suitable host matrix for TE additives, as it can naturally sustain the temperature gradients necessary for power generation [27,28]. Previous research has explored the creation of TE cement by incorporating various conductive fillers, including carbon fibers, CNT, graphite, and graphene [29–31]. CNT have emerged as particularly effective TE fillers for cement, owing to their high aspect ratio, electrical/thermal conductivities, and mechanical robustness [32,33]. Notably, Tzounis et al. realized p- and n-type cement/CNT nanocomposites and demonstrated a structural TE generator, establishing the viability of cement-based TE devices for harvesting low-grade heat in the built environment [34]. Wei et al. showed that compression-shear-fabricated CNT/cement composites exhibit measurable Seebeck response once a conductive CNT network forms within the matrix [35].

However, a persistent and critical challenge has impeded progress; the effective dispersion of CNT within the cementitious matrix. Due to strong van der Waals forces and their hydrophobic nature, CNT tend to form tightly bound agglomerates in the aqueous, high-pH (typically >12) environment of fresh cement paste [36]. These agglomerates not only fail to form an efficient, interconnected conductive network but also act as defect sites, compromising the mechanical integrity of the final composite. While various dispersion techniques have been attempted, including ultrasonication and the use of conventional surfactants, achieving a stable and homogeneous dispersion that survives the mixing and hydration process remains a significant hurdle [37,38].

This study proposes a novel strategy to overcome the fundamental dispersion challenge and simultaneously enhance the TE performance of cement composites. The objective of this work is to systematically fabricate, characterize, and analyze these novel PEDOT:PSS/MWNT-cement composites. By evaluating their microstructural features, TE properties (σ and S), and mechanical performance (compressive strength), we aim to elucidate the underlying physical and chemical mechanisms that govern their behavior. This approach offers a scalable, water-based method for developing the next generation of smart, energy-harvesting construction materials.

2. Materials and methods

2.1. Materials

The primary binder used in this study was Type 1 ordinary Portland cement (OPC), supplied by Sampyo Cement, Korea, with a measured density of 3.13 g/cm^3 and a Blaine fineness of 3820 cm^2/g. Natural sand, conforming to standard specifications with a density of 2.60 g/cm^3, a fineness modulus of 2.45, and a water absorption rate of 1.0 %, was used as the fine aggregate. The conductive nanocomposite suspension was prepared using multi-walled carbon nanotubes (MWNT) and a commercial aqueous dispersion of PEDOT:PSS (Clevios PH1000, Heraeus), which has a solid content of approximately 2.0 wt% in water.

2.2. Synthesis of PEDOT:PSS/MWNT-cement composites

A series of TE cement composites were prepared with varying MWNT concentrations. The synthesis procedure is depicted schematically in Fig. 1. For each batch, a predetermined mass of MWNT, corresponding to 0.25, 0.50, 0.75, and 1.0 wt% of the total cement mass, was added to the PEDOT:PSS aqueous solution. To achieve a homogeneous and stable dispersion of the nanotubes, prior to ultrasonication, the MWNT powder was manually ground with a mortar and pestle for approximately 10 min in the PEDOT:PSS aqueous medium to promote wetting and disintegr1ation of large aggregates. Then, MWNT suspensions were bath-sonicated for 30 min to pre-disperse agglomerates. Subsequently, the suspensions underwent probe sonication at 40 W for 30 min while being maintained in an ice–water bath to prevent the temperature from exceeding 30 °C and to minimize CNT shortening or structural damage. Finally, the dispersions were subjected to an additional 30 min of bath sonication under the same conditions to ensure complete homogenization of MWNT within the PEDOT:PSS matrix. This sequential bath–probe–bath protocol was selected to combine the gentle de-agglomeration of bath sonication with the more intense localized energy of probe sonication, yielding stable, uniformly dispersed MWNT/PEDOT:PSS mixtures suitable for subsequent cement composite preparation. A control sample (plain) without any conductive additives was also prepared for baseline comparison. The fabrication process began with the dry mixing of OPC and sand for approximately 2 min to ensure uniformity. Subsequently, the prepared PEDOT:PSS/MWNT aqueous suspension was added to the dry mixture. The entire batch was then mixed for an additional 5 min in a mechanical mixer to form a homogeneous and workable mortar. The water-to-cement ratio was maintained at 0.5 for all formulations. Control samples were prepared using water, cement, and natural fine aggregate, ingredients commonly used in cement composites. Specifically, the control sample was prepared by mixing cement and sand for 2 min, then adding water and mixing for 5 min, following the same process used to prepare PEDOT:PSS/MWNT composites.

2.3. Specimen preparation and curing

The fresh mortar was cast into acrylic molds of three different geometries to facilitate specific characterization tests; cubic specimens (50 × 50 × 50 mm) for compressive strength testing, bar-shaped

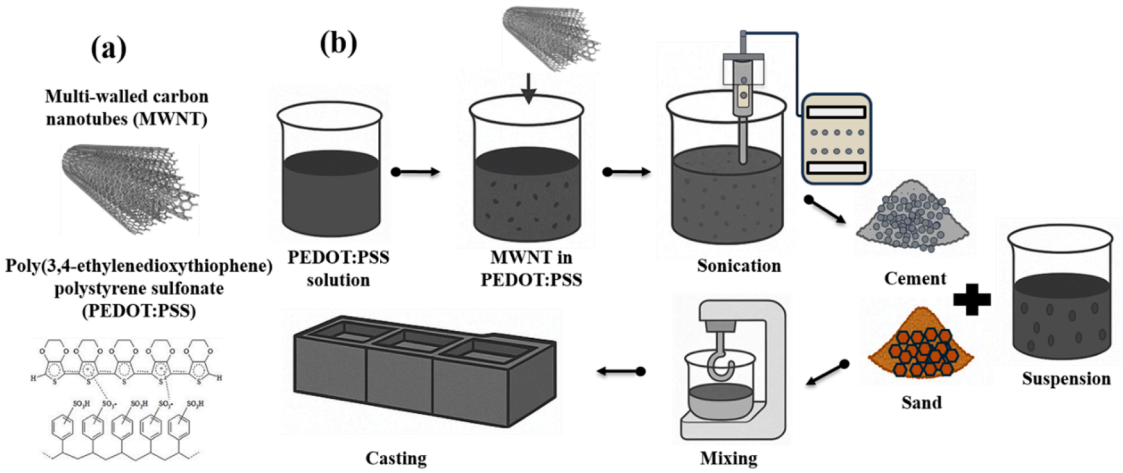

Fig. 1. (a) Chemical structures of MWNT and PEDOT:PSS, and (b) Schematic illustration of the preparation process for PEDOT:PSS/MWNT-cement composites. MWNT were dispersed in aqueous PEDOT:PSS by a sequential bath–probe–bath sonications, followed by mixing with cement and sand at a water-to-cement ratio of 0.5. The resulting mortars were cast into molds and cured under conditions described in Section 2.3.

specimens (20 × 20 × 200 mm) for TE property measurements, and coin-shaped specimens (20 mm diameter, 10 mm thickness) for thermal conductivity measurements. Table 1 summarizes the concentrations of the components (*i.e.*, MWNT, PEDOT:PSS, sand, cement, and D.I water) of the fabricated composites material samples. The detailed process of specimen production is provided in Supporting Information (Fig. S1). After casting, all specimens were stored at room temperature for 24 h to allow for initial setting. Following this period, the specimens were demolded. To ensure proper hydration and strength development, the cubic specimens designated for mechanical testing were cured in a humidity chamber at 20 °C and 100 % relative humidity for 28 days. In contrast, the bar and coin specimens for TE and thermal property evaluation were stored at ambient room temperature and humidity to minimize the influence of free moisture on the electrical and thermal measurements.

2.4. Characterization

The internal microstructure of the hardened composites and the dispersion state of the MWNT were examined using a field emission scanning electron microscope (FE-SEM, S-4800 Hitachi, Japan) at the Core Facility for Supporting Analysis & Imaging of Biomedical Materials at Wonkwang University supported by National Research Facilities and Equipment Center. Samples for FE-SEM analysis were obtained from the fractured surfaces of specimens after compressive strength testing. Energy-dispersive X-ray spectroscopy (EDX, Oxford Instruments, UK) was performed to determine elemental composition. The fragments were mounted on aluminum stubs and sputter-coated with a thin layer of gold to ensure surface conductivity before imaging. Images were captured at various magnifications using an accelerating voltage of 15 kV. The σ and S were measured on the bar-shaped specimens using a custom-built, shielded four-point probe apparatus. The setup, controlled via LabVIEW, integrates a Keithley 2000 Multimeter and a PPS-3635 power supply. The electrical resistance R of the specimen was determined from the slope of the current-voltage (I-V) characteristic curve, which was measured at multiple voltage levels (e.g., 5 V, 7 V, and 10 V) to ensure linearity and accuracy. The σ was then calculated using the formula $\sigma = L/(R \bullet A)$, where L is the distance between the inner voltage probes and A is the cross-sectional area of the specimen (20 × 20 mm). To measure the S, a temperature gradient ($\Delta T = T_{hot} - T_{cold}$) was established along the longitudinal axis of the bar specimen using two Peltier elements attached to its ends. One element acted as a heater and the other as a cooler. The temperature at each end was monitored precisely using K-type thermocouples. The resulting thermoelectric voltage (ΔV) generated by the Seebeck effect was measured across the same thermocouple leads. The S was determined from the slope of the linear relationship between ΔV and ΔT over a series of six to eight temperature steps. The K of the composite material was evaluated based on the one-dimensional heat conduction framework governed by Fourier's law. A custom-built apparatus conforming to ASTM D5470 standards (Fig. S2) was employed to measure thermal conductivity in the through-thickness direction of the specimen. According to the ASTM D5470 protocol, K is determined using parameters such as the heat flow rate (Q), cross-sectional area of the sample (A), temperature gradient across the specimen (ΔT), and its thickness (L).

$$Q_{bar} = K_{bar} A \frac{\Delta T_{bar}}{\Delta L_{bar}} \tag{1}$$

$$Q_{bar} = Q_{sample} \tag{2}$$

$$Q_{sample} = \frac{Q_{sample}}{A} \frac{\Delta L_{sample}}{\Delta T_{sample}} \tag{3}$$

Heating and cooling sources were attached to the lower and upper metal rods, respectively, while the ASTM-standardized coin-shaped specimens were sandwiched between them. The entire assembly was maintained under steady conditions until thermal equilibrium was reached to ensure stable heat transfer through the sample. A series of thermocouples embedded in the metal rods were used to monitor the temperature distribution along their lengths. The heat flow through the metal rods was calculated using Eq. (1), and the temperature drop across the sample was estimated via linear interpolation between the thermocouple readings. Assuming one-dimensional steady-state conduction, the heat flux through the specimen was considered equal to that through the metal rods (Eq. (2)). Consequently, the thermal conductivity of the sample was derived using Eq. (3). To minimize the contact thermal

Table 1
Specimen components.

Type (mm)	MWNT (wt%)	MWNT (g)	PEDOT:PSS (g)	D.I water (g)	Cement (g)	Sand (g)
Cube (50x50x50mm)	0	0	0	74	147	320
	0.25	0.19	7.4	66.6		
Coin (Ø30x20mm)	0.5	0.37	7.4	66.6		
	0.75	0.56	7.4	66.6		
Bar (20x20x200mm)	1.0	0.74	7.4	66.6		

resist, specimen faces were sanded to achieve flat parallel surfaces prior to measurement. A thin layer of high-conductivity thermal grease was applied to both interfaces to expel air gaps. The specimen was clamped between meter bars under an applied force of 11–12 kgf (Bongshin BS-205 load indicator), corresponding to a contact pressure of 0.15–0.17 MPa (22–24 psi) for a 30 mm diameter specimen. This pressure range was selected as it provides stable thermal contact without specimen slippage or mechanical damage. The upper and lower bar gradients were compared, and the difference was always within 10 %, confirming near-uniform heat flux across the specimen thickness. To ensure reliable TE measurements, all experiments were conducted under steady-state conditions. The temperature difference (ΔT) across the specimen was monitored continuously, and data acquisition was initiated only after the fluctuation in ΔT was less than ± 0.1 K for at least 5 min. This criterion was applied consistently for σ, S and k measurements. The 28-day compressive strength of the cubic specimens was determined in accordance with the KS L 5105 standard, which is analogous to ASTM C109. The tests were performed using an MTS 815 concrete compression tensile tester with a maximum load capacity of 980 KN. For each composition, three independent specimens were prepared for thermoelectric and mechanical property evaluation. TE properties (σ, S, and k) and compressive strength were each measured three times per specimen, and the reported values represent the average of these measurements. Standard deviations are presented as error bars in the corresponding figures to indicate data variability and measurement reproducibility.

3. Results and discussion

3.1. Microstructure and nanofiller dispersion

The efficacy of any nanocomposite material is fundamentally governed by the dispersion quality of the nanofiller within the host matrix [39,40]. In cementitious systems, achieving homogeneous dispersion is particularly challenging but is a prerequisite for realizing enhanced properties [41–43]. The dispersion stability of MWNT in PEDOT:PSS solution was clearly demonstrated by a photo-image taken after sonication and centrifugation processes, as shown in Fig. S3. The lack of visible aggregation indicates that PEDOT:PSS plays a crucial role in maintaining colloidal stability, a behavior consistent with previous reports on carbon nanotube-based hybrid dispersions. Further characterization using AFM and SEM of dilute drop-cast samples on Si-wafers revealed a well-dispersed network of carbon nanotubes within the negatively charged polymer matrix. The observed uniformity and minimal bundling imply that PEDOT:PSS acts as an effective dispersant, suppressing van der Waals-induced aggregation and promoting the stable integration of MWNT into cement-based composite systems. The PEDOT:PSS/MWNT dispersion prepared via the bath-tip-bath sonication sequence remained visually stable without sedimentation for over three weeks at ambient conditions. SEM examination of a Si-wafer sample drop-cast from the aged suspension confirmed that MWNT remained uniformly distributed with no significant aggregation, comparable to the freshly prepared suspension (Fig. S4). This long-term stability can be attributed to the synergistic effects of π–π interactions between MWNT and PEDOT, and electrostatic repulsion from the PSS sulfonate groups.

Fig. 2 presents a series of SEM micrographs of the fractured surfaces of the PEDOT:PSS/MWNT-cement composites at varying MWNT concentrations. At lower concentrations of 0.25 wt% (Fig. 2a) and 0.5 wt% (Fig. 2b), the MWNT appear to be well-dispersed throughout the cementitious matrix. Individual nanotubes and small, untangled bundles can be seen embedded within and bridging the calcium-silicate-hydrate (C-S-H) gel, which is the primary binding phase in hardened cement [44, 45]. This uniform distribution is critical, as it allows for the formation of a continuous, three-dimensional network necessary for both electrical conduction and mechanical reinforcement. However, as the MWNT content increases to 0.75 wt% (Fig. 2c) and further to 1.0 wt% (Fig. 2d), the onset of agglomeration became evident. In these samples, larger, more densely packed clusters of entangled nanotubes are observed. These agglomerates represent regions of poor dispersion where the van der Waals forces between the nanotubes have overcome the stabilizing effect of the dispersing agent. The successful dispersion observed at lower concentrations can be directly attributed to the dual-functionality of the PEDOT:PSS suspension. Bare CNT are notoriously hydrophobic and readily bundle together in the aqueous, high-ionic-strength environment of cement paste [46]. The PEDOT:PSS complex, consisting of a hydrophobic, conjugated PEDOT core and a hydrophilic, anionic PSS

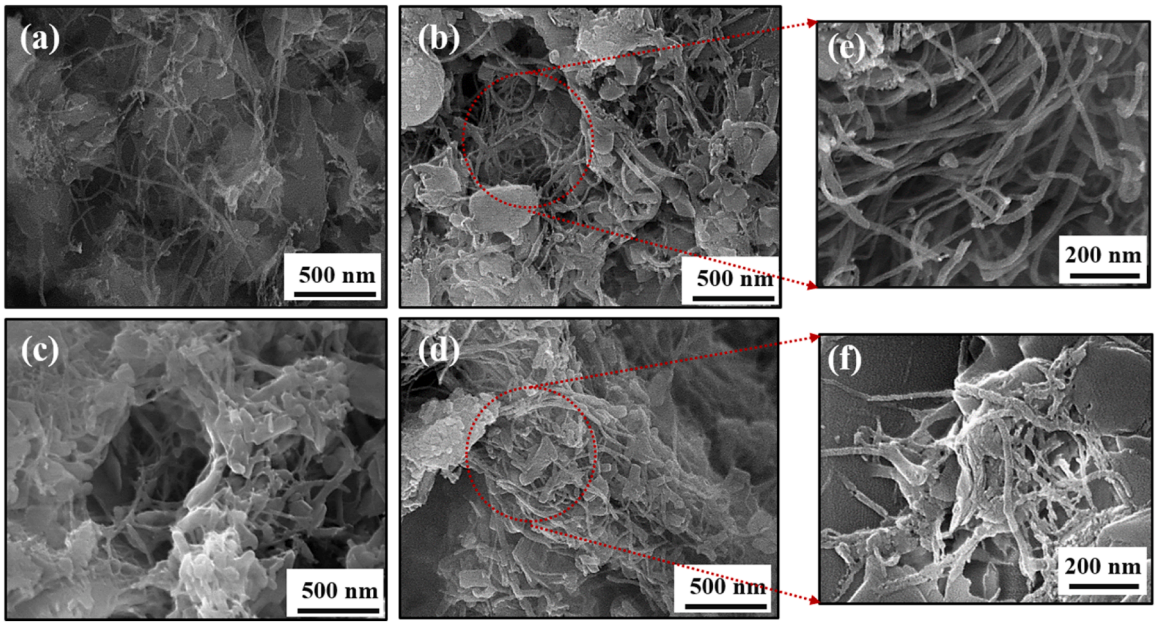

Fig. 2. SEM images of PEDOT:PSS/MWNT-cement composites with MWNT contents of (a) 0.25 wt%, (b) 0.5 wt%, (c) 0.75 wt%, and (d) 1.0 wt%. Image (e) is a magnified view that highlights the high dispersion of nanotubes forming a network structure within the cement matrix at 0.5 wt%. In contrast, image (f) clearly shows significant aggregation and poor dispersion of nanotubes at the higher 1.0 wt% concentration.

shell, acts as a powerful polymeric surfactant. During the initial sonication step, the PEDOT core is believed to adsorb onto the graphitic surface of the MWNT via non-covalent π-π stacking interactions [47]. This encapsulates the nanotubes within a shell of negatively charged, hydrophilic PSS chains that extend into the surrounding water. This process provides robust electrostatic stabilization, effectively preventing the nanotubes from re-agglomerating both in the initial suspension and during the subsequent mixing with the cement powder. The SEM evidence strongly suggests that this novel dispersion strategy is highly effective up to a concentration of approximately 0.5 wt%, beyond which the quantity of nanotubes begins to exceed the stabilizing capacity of the fixed amount of PEDOT:PSS used. Additional high-resolution SEM images and corresponding EDX elemental maps of the TE-1.0 sample, confirming the coexistence of cement hydration phases (Ca, Si, Al, K) and sulfur originating from PEDOT:PSS, are provided in the Supporting Information (Fig. S5). These results further substantiate that CNT agglomeration and heterogeneous organic–inorganic interfaces at higher loadings are responsible for enhanced phonon scattering and the reduction in thermal conductivity.

3.2. Electrical property

The thermoelectric performance of the composites was evaluated by measuring their electrical conductivity (σ) and Seebeck coefficient (S). The results, plotted as a function of MWNT content, are shown in Fig. 3. The σ exhibits a clear and significant dependence on the MWNT concentration. Hereafter, TE-0.25, TE-0.5, TE-0.75, and TE-1.0 refer to cement composites containing 0.25, 0.5, 0.75, and 1.0 wt% MWNT, respectively, dispersed in PEDOT:PSS solution. A pronounced increase in σ is observed between TE-0.25 (1.20×10^{-2} S/m) and TE-0.5 (5.19×10^{-2} S/m), indicating that the percolation threshold for MWNT dispersion within the cement matrix is approached near 0.5 wt%. This ~4.3-fold enhancement confirms the successful formation of an interconnected conductive network throughout the cement matrix. Beyond this point, σ remains nearly constant (5.39×10^{-2} S/m for TE-0.75 and 5.73×10^{-2} S/m for TE-1.0), indicating that an interconnected conductive network has already formed and that further MWNT addition yields marginal conductivity gains. This plateau behavior is consistent with percolation theory, in which a sharp conductivity increase at the threshold is followed by a saturation regime once the conductive pathways are fully established. Notably, unlike typical CNT/insulator cement composites reported in the literature, which often exhibit an abrupt, orders-of-magnitude increase in conductivity at the percolation threshold, our system shows a more moderate enhancement of about five-fold between TE-0.25 and TE-0.5 [48]. This sharp yet comparatively smaller jump suggests that while a percolation threshold is reached around 0.5 wt% MWNT, the initial conductivity at 0.25 wt% is already significant due to the presence of a pre-existing conductive PEDOT:PSS network within the cement matrix. In this "double percolation" scenario, PEDOT:PSS forms a continuous, conductive phase that enables charge transport even at the lowest MWNT loading, and the addition of MWNT primarily serves to densify and optimize the conductive pathways rather than transition from a fully insulating to a conductive state. This mechanism explains the pronounced increase at 0.5 wt% followed by the conductivity plateau at higher filler contents. The evolution of σ with increasing MWNT content follows a classical percolation-type behavior. To quantify the percolation threshold (ϕ_c), critical exponent (t), and σ data were analyzed using the scaling law of percolation theory, $\sigma = \sigma_o (\phi - \phi_c)^t$, where σ_o is the prefactor related to intrinsic nanotube conductivity and network connectivity, and ϕ is the MWNT loading fraction. A nonlinear regression of the experimental σ values (0.25–1.0 wt%) yielded $\phi_c \approx 0.47$ wt% and $t \approx 1.9$, indicating the formation of a three-dimensional conductive pathway within the cementitious matrix. The obtained t value aligns well with typical 3D percolation systems [49]. Below this threshold, isolated MWNT clusters act as discrete charge islands with limited interconnection, resulting in low σ. Once ϕ exceeds ϕc, PEDOT:PSS bridges neighboring MWNT, drastically reducing tunneling resistance and enabling a continuous charge transport network. Beyond 0.5 wt%, σ approaches a plateau due to network saturation and increased tube–tube junction scattering. These results confirm that the electrical percolation threshold of the PEDOT:PSS/MWNT-cement composite occurs near 0.5 wt%, validating the percolation-controlled conduction mechanism.

In contrast to the σ, the S shows a non-monotonic relationship with MWNT content (Fig. 3b). The highest S, approximately 16 μV/K, is observed for the TE-0.5 sample. As the MWNT concentration increases from this peak, the S systematically decreases, falling to approximately 13 μV/K at 1.0 wt%. The positive sign of the S across all samples confirms that the composites behave as p-type thermoelectric materials, where holes are the majority charge carriers. This trend can be understood by considering the composite as a system with two competing conductive pathways. PEDOT:PSS is a known p-type TE material with a relatively high intrinsic S (often exceeding 20 μV/K). MWNT, while highly conductive, generally exhibit a much lower S. At low MWNT concentration (e.g., 0.5 wt%), charge transport is predominantly governed by the PEDOT:PSS matrix, resulting in a higher overall S. As the concentration of highly conductive MWNT increases, they provide a path of lower electrical resistance. A greater fraction of the charge carriers flows through these low-resistance nanotube pathways, effectively reducing the volume-averaged S of the composite. The observed

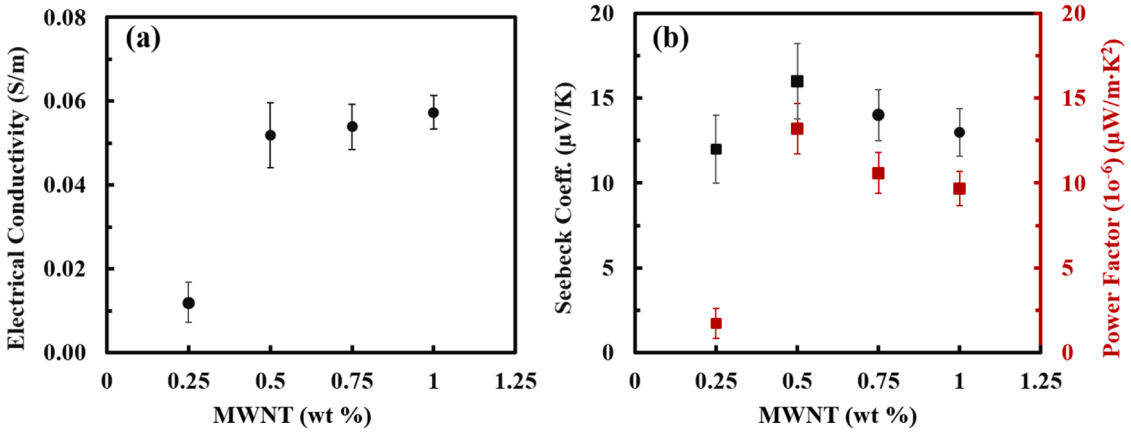

Fig. 3. (a) Electrical conductivity (σ) and (b) Seebeck coefficient (S, black circles) with corresponding power factor (PF, red squares) of PEDOT:PSS/MWNT cement composites as a function of MWNT content (0–1.0 wt%). Each data point represents the mean of three independently prepared bar specimens, with error bars indicating standard deviations.

non-monotonic behavior of the S with increasing MWNT loading can be rationalized by the interplay of two competing mechanisms. At low to moderate MWNT concentrations, the interfaces between MWNT and PEDOT:PSS act as energy filtering barriers that selectively transmit high-energy charge carriers, leading to an increase in S. This enhancement is further supported by the improved alignment and dispersion of MWNT, which facilitates anisotropic transport pathways. However, beyond ~0.5 wt% MWNT, the density of inter-tube contacts rises, effectively reducing the number and potential height of PEDOT:PSS-MWNT junction barriers. This reduction in energy filtering, combined with the increased carrier concentration from the highly interconnected conductive network, results in a slight decline in S at higher MWNT loadings. The ultimate measure of electrical performance for a TE material is the power factor, $PF = S^2 \bullet \sigma$. As shown in Fig. 3(b), the interplay between the increasing σ and decreasing S results in an optimal composition for the PF. The highest PF of approximately 1.33×10^{-5} $\mu W/mK^2$ is achieved for the TE-0.5 sample. These results indicate that for energy harvesting applications, lower concentrations of well-dispersed MWNT in a PEDOT:PSS matrix are more effective than higher, more conductive loadings where the S is compromised.

3.3. Thermal conductivity

The thermal conductivity (k) of the composites, as depicted in Fig. 4, exhibits a non-monotonic relationship with the MWNT content. Initially, the k increases from approximately 0.82 W/m·K for the plain matrix to a peak value of 1.12 W/m·K at an optimal MWNT concentration of 0.5 wt %. Beyond this point, as the MWNT content is further increased to 0.75 wt% and 1.0 wt%, the k decreases, settling at a value of approximately 0.94 W/m·K. This complex behavior can be understood as a competition between two opposing effects: the formation of heat-conductive pathways and the proliferation of phonon-scattering interfaces. At lower concentrations ($\leq$ 0.5 wt%), the MWNTs are well-dispersed throughout the cementitious matrix, as confirmed by the microstructural analysis. Given the intrinsically high thermal conductivity of individual MWNT, these dispersed nanotubes begin to form an effective network for heat transport, leading to an initial enhancement of the composite's overall k compared to the plain cement. However, as the MWNT concentration increases beyond the optimal dispersion threshold of 0.5 wt%, the dominant mechanism shifts. The decrease in k at higher loadings ($\geq$ 0.75 wt%) is primarily attributed to the significant increase in interfacial thermal resistance, also known as Kapitza resistance. At low MWNT loadings ($\leq$ 0.25 wt%), the absence of continuous nanotube pathways results in heat transport being dominated by the cement and PEDOT:PSS phases, which possess relatively low k values. Upon approaching the percolation threshold (~0.5 wt%), the formation of interconnected MWNT networks significantly enhances phonon transport, leveraging the high intrinsic k of MWNT (~2000–3000 W/m·K). Beyond this concentration, additional MWNT further densify the network but yield smaller k increments, likely due to increased phonon scattering at nanotube junctions, defect sites, and polymer interfaces.

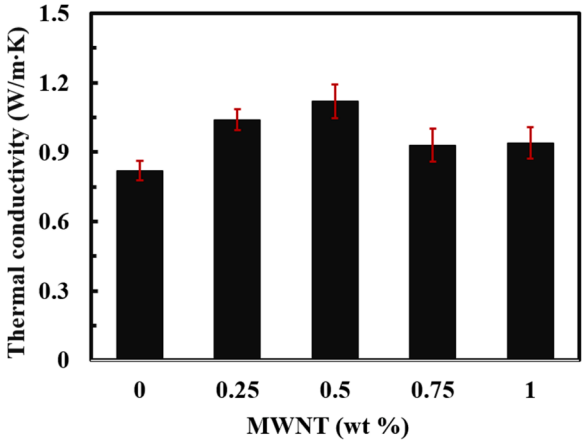

Fig. 4. Non-monotonic thermal conductivity (k) of the cement composites with varying MWNT content. The data shows that conductivity peaks at 1.12 W/m·K for the 0.5 wt% sample, indicating an optimal concentration before the effects of phonon scattering at higher loadings become dominant. All data points represent the mean values obtained from three independent specimens, with each specimen measured three times.

Heat in the composite is predominantly carried by phonons (quantized lattice vibrations). These phonons are effectively scattered at the numerous interfaces between dissimilar materials within the composite, particularly at the junctions between the hard, inorganic C-S-H matrix and the soft, amorphous PEDOT:PSS polymer coating, due to a severe acoustic impedance mismatch. Crucially, at higher concentrations, the MWNT begin to form agglomerates. These clusters introduce a high density of nanotube-nanotube junctions and voids, which act as potent sites for phonon scattering. This intense scattering disrupts coherent heat flow and impedes thermal transport more than the addition of conductive material enhances it. Therefore, while electrons can transpose junctions relatively easily to increase σ, phonons are scattered, effectively decoupling thermal transport from electrical transport. The peak k at 0.5 wt% thus represents the optimal balance, where a sufficient conductive network is formed without the overwhelming negative impact of phonon scattering caused by agglomeration.

3.4. Thermoelectric figure of merit

Table 2 summarizes the σ, k, and ZT corresponding to various CNT contents in the cement-based composites, along with comparisons to values reported in the literature. In this study, key parameters such as σ, S, PF, k, ZT, and mechanical strength were comprehensively evaluated to assess the feasibility of the composites as both structural and functional materials. While similar levels of MWNT incorporation in prior studies have yielded comparable or slightly improved electrical properties, those studies often focused on only a subset of performance indicators, such as σ for TE applications or compressive strength for structural analysis. Moreover, although higher MWNT loadings or alternative additives have demonstrated superior electrical properties, they frequently compromise cost-effectiveness. Therefore, the integrated thermoelectric evaluation conducted on composites containing 0.5 wt% MWNT in this work provides meaningful insights and practical benchmarks for the development of multifunctional cementitious materials aimed at structural energy harvesting applications.

The calculated ZT values for the composites as a function of MWNT content are presented in Fig. 5. The results demonstrate a clear optimal concentration for TE performance, with the ZT value reaching a peak of 3.53×10^{-9} at 0.5 wt% MWNT content. This non-monotonic trend in ZT is the result of the complex interplay between the electrical and thermal transport properties of the composite. The numerator of the ZT equation, the PF, is itself governed by competing trends. As previously established, the σ increases monotonically with MWNT loading, rising by a factor of nearly five from 0.25 wt% to 1.0 wt%. In contrast, the S peaks at 0.5 wt % before decreasing at higher concentrations. The synergistic combination of these two factors results in the PF also peaking at the 0.5 wt% concentration, where it increases by more than 7.2 times compared to the 0.25 wt% sample. The peak ZT value at 0.5 wt% is achieved because the substantial enhancement in the PF far outweighs the modest increase in k in this concentration range. Beyond this optimal point, the decrease in both the S and k results in a slight reduction of the overall ZT. This analysis confirms that the 0.5 wt% MWNT concentration represents the optimal balance of all contributing TE parameters, maximizing the material's potential for energy conversion and reinforcing its status as the ideal composition for achieving synergistic multifunctionality.

Table 2
Summary of thermoelectric properties of carbon nanomaterials-reinforced cement composites at various loadings, compared with reported values from prior literature.

Fillers	σ (S/m)	S (μV/K)	PF (μW/m•K^2)	k (W/m•K)	ZT	MPa	Ref.
MWNT 0.25 wt%/PEDOT:PSS	1.20×10^{-2}	12	1.72×10^{-6}	1.04	4.94×10^{-10}	32.3	Current
MWNT 0.5 wt%/PEDOT:PSS	5.19×10^{-2}	16	1.33×10^{-5}	1.12	3.53×10^{-9}	33.1	study
MWNT 0.75 wt%/PEDOT:PSS	5.39×10^{-2}	14	1.06×10^{-5}	0.93	3.39×10^{-9}	25.0	
MWNT 1.0 wt%/PEDOT:PSS	5.73×10^{-2}	13	9.68×10^{-6}	0.74	3.07×10^{-9}	30.6	
W/C 0.2, MWCNT 0.15 vol%		260.3					[50]
W/C 0.2, MWCNT 0.30 vol%	5×10^{-3}	147.5	0.11×10^{-3}				
W/C 0.2, MWCNT 0.50 vol%		330.4				76.9	
W/C 0.3, MWCNT 0.15 vol%		132.4					
W/C 0.3, MWCNT 0.30 vol%	15.5×10^{-3}	345.2	1.79×10^{-3}				
W/C 0.3, MWCNT 0.50 vol%		743				53.5	
W/C 0.4, MWCNT 0.15 vol%		331					
W/C 0.4, MWCNT 0.30 vol%	53.2×10^{-3}	86.7	0.4×10^{-3}				
W/C 0.4, MWCNT 0.50 vol%		149.1				34.3	
W/C 0.5, MWCNT 0.15 vol%		324					
W/C 0.5, MWCNT 0.30 vol%	138×10^{-3}	52.7	0.93×10^{-3}				
W/C 0.5, MWCNT 0.50 vol%		18.37				22.4	
MWCNT 0.1 wt%							[51]
MWCNT 0.6 wt%							
MWCNT 0.9 wt%							
MWCNT 1.0 wt%	4.79 × 105						
MWCNT 0.1 vol%						58.1	[52]
MWCNT 0.2 vol%						58.6	
MWCNT 0.3 vol%						56.2	
MWCNT 0.4 vol%						56.0	
MWCNT 0.5 vol%						55.9	
MWCNT 5 wt%	4.00 × 10	40	6.40×10^{-3}	0.73	2.63×10^{-6}		[53]
MWCNT 10 wt%	3.00 × 101	50	7.50×10^{-2}	0.84	2.68×10^{-5}		
MWCNT 15 wt%	8.20 × 101	53	2.30×10^{-1}	0.95	7.27×10^{-5}		
MWCNT 0.0625 wt%	1.42×10^{-6}			2.09		33.69	[54]
MWCNT 0.1 wt%	7.83×10^{-4}			2.01		31.18	
MWCNT 0.125 wt%	3.04×10^{-3}	14.45	6.35×10^{-7}	1.95	9.78×10^{-11}	30.00	
MWCNT 0.2 wt%	5.56×10^{-3}	15.41	1.32×10^{-6}	1.91	2.07×10^{-10}	30.83	
MWCNT 0.25 wt%	2.52×10^{-2}	13.67	4.71×10^{-6}	1.89	7.48×10^{-10}	31.24	
CF 1.2 wt%			1.85×10^{-4}	1.24	2.22×10^{-7}		[55]
GnP 10 wt%		30		0.94	0.025×10^{-2}		[56]
Gnp 10 wt%/Fe_2O_3 10 wt%		105		0.66	0.5×10^{-2}		
Gnp 10 wt%/ZnO 10 wt%		140		0.95	1.0×10^{-2}		
Gnp 10 wt%/MnO_2 10 wt%		100		0.90	0.2×10^{-2}		
GO 0 wt%							[57]
GO 0.05 wt%							
GO 1.0 wt%				0.77			
GO 2.0 wt%							
GO 4.0 wt%							

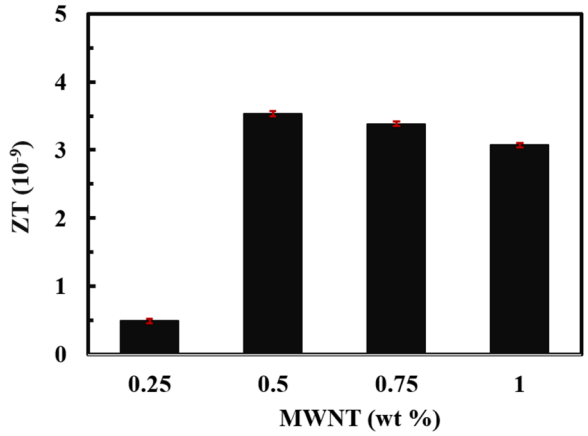

Fig. 5. The dimensionless thermoelectric figure of merit, ZT, of the composites as a function of MWNT content. The ZT value is calculated from the measured electrical conductivity (σ), Seebeck coefficient (S), and thermal conductivity (k) using the equation, $ZT = (\sigma \bullet S^2/k)T$. All data points represent the mean values obtained from three independent specimens, with each specimen measured three times.

3.5. Mechanical properties

For a TE material to be viable for infrastructure applications, it must not only exhibit functional properties but also maintain or enhance the structural integrity of the host material. Fig. 6 presents the 28-day compressive strength of the composites. The plain cement mortar exhibited a baseline strength of 27.7 MPa. The addition of the PEDOT:PSS/MWNT suspension resulted in a significant improvement in mechanical performance at lower concentrations. The compressive strength increased to 32.3 MPa for the TE-0.25 sample and reached a peak value of 33.1 MPa for the TE-0.50 sample, representing a notable 19.5 % enhancement over the control. This strengthening effect can be attributed to several synergistic nanomechanical reinforcement mechanisms. First, the well-dispersed nanoparticles act as fillers, physically occupying nanoscale voids and pores within the cement matrix, leading to a denser microstructure. As nanoscale voids and pores are filled, the denser microstructure can improve compressive strength by suppressing the formation of pores that negatively affect compressive strength [58]. s, the high surface area of the nanotubes provides abundant nucleation sites for the growth of C-S-H gel, accelerating hydration and promoting the formation of a more robust and interconnected solid phase. This phenomenon is similar to results reported in existing literature [59,60]. Finally, the high-aspect-ratio nanotubes act as reinforcing fibers at the nanoscale, effectively bridging emergent nano- and micro-cracks, which dissipates fracture energy and arrests crack propagation, thereby

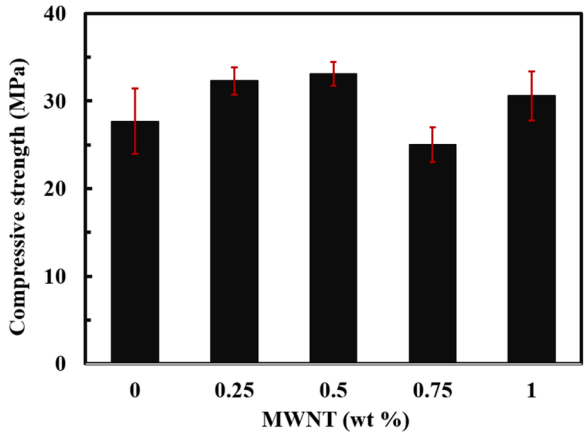

Fig. 6. 28-day compressive strength of PEDOT:PSS/MWNT cement composites as a function of MWNT content (0–1.0 wt%). Cubic specimens (50 × 50 × 50 mm) were prepared and tested according to KS L 5105 (analogous to ASTM C109). Values represent the mean of three independent specimens, and error bars denote standard deviations. The optimal reinforcement effect is observed at 0.5 wt% MWNT, yielding a 19.5 % increase compared with plain cement.

increasing the overall strength and toughness of the composite [61]. However, beyond the optimal concentration of 0.5 wt%, the mechanical performance degrades. The compressive strength drops sharply to 25.0 MPa for the TE-0.75 sample, which is lower than that of the plain cement. This decline in strength correlates directly with the onset of nanotube agglomeration observed in the SEM analysis (Fig. 2c). These poorly dispersed CNT bundles act as stress concentration points and create weak, porous zones within the matrix, negating the benefits of nanoreinforcement and leading to premature failure under load. Although the strength recovers slightly to 30.6 MPa for the TE-1.0 sample, it remains below the peak performance, confirming that 0.5 wt% represents the optimal balance between reinforcement and agglomeration effects.

The observed 19.5 % improvement in compressive strength at 0.5 wt % MWNT arises from the complementary roles of PEDOT:PSS and MWNT. PEDOT:PSS uniformly coats hydration products, filling microvoids and refining the microstructure, while MWNT bridge microcracks and enhance stress transfer efficiency. Together, these effects result in a denser, more mechanically robust cement matrix. In terms of TE properties, PEDOT:PSS provides an initial conductive phase within the cement pores, enabling efficient carrier transport even at low MWNT loadings. As MWNT content increases to the percolation threshold (~0.5 wt%), a continuous hybrid network forms, simultaneously maximizing σ and preserving a favorable S. This balance explains the peak PF at 0.5 wt% MWNT and highlights the critical role of the synergistic interaction between PEDOT:PSS and MWNT in optimizing both mechanical and TE performance. Despite these advantages, the highest compressive strength achieved in this study was approximately 33.1 MPa, which is slightly below the 40 MPa threshold typically required for high-performance cementitious composites. To further enhance the mechanical performance while maintaining thermoelectric functionality, future research will focus on optimizing the water-to-cement ratio (reducing it below the current 0.50) and incorporating mineral admixtures such as ground granulated blast furnace slag and fly ash, which are known to refine the microstructure and improve long-term strength development.

3.6. *Interfacial engineering for synergistic multifunctionality*

An aqueous suspension of the conductive polymer PEDOT:PSS can serve as a highly effective, multifunctional additive for creating high-performance MWNT-cement composites. PEDOT:PSS serves a dual role in the PEDOT:PSS/MWNT-cement composites. Mechanically, the sulfonate-rich PSS chains adsorb onto MWNT surfaces through π-π interactions, while extending hydrophilic domains into the aqueous phase to impart electrostatic and steric stabilization, thereby preventing re-agglomeration during mixing. Electrochemically, the PEDOT backbone is intrinsically conductive, bridging adjacent MWNTs and lowering inter-tube contact resistance, while PSS domains maintain electrical conductivity in the alkaline cement pore solution. The PEDOT:PSS/MWNT interface may also promote an energy-filtering effect, scattering low-energy carriers and enhancing the S. This dual function results in improved MWNT dispersion, increased σ, and optimized thermoelectric performance, as confirmed by microstructural and electrical measurements. The PEDOT:PSS polyelectrolyte complex, with its hydrophobic PEDOT core and hydrophilic PSS shell, is expected to adsorb onto the surface of MWNT [62]. This process, driven by π-π interactions and facilitated by sonication, creates a stabilizing layer that prevents re-agglomeration through a combination of steric and electrostatic repulsion, ensuring a homogeneous distribution of nanotubes within the cement paste. Unlike inert surfactants, PEDOT:PSS is itself a p-type thermoelectric material. By coating the MWNT and filling the interstitial spaces, it can form a continuous hybrid conductive network, creating additional pathways for charge transport and contributing positively to the overall S and PF of the composite. The superior performance of the PEDOT:PSS/MWNT-cement composites stems from a combination of unique physical and chemical mechanisms at the nanoscale. The electrical properties are governed by a double percolation network, where charge carriers can move through both the p-type PEDOT:PSS polymer phase and the highly conductive MWNT network [63]. This hybrid system provides robust conductivity without the sharp, often unreliable, percolation threshold seen in simple insulator-conductor composites. CNT are intrinsically excellent thermal conductors [64].

However, in a composite, the overall thermal transport is dominated by interfacial thermal resistance (also known as Kapitza resistance) [65]. Phonons (quantized lattice vibrations that carry heat) must traverse these multiple boundaries, each characterized by a significant acoustic impedance mismatch. The soft, amorphous polymer layer is particularly effective at scattering phonons, disrupting coherent heat flow, as shown in Fig. 7. This effective decoupling of high σ from k is the cornerstone of designing high-performance TE materials.

The stability of the dispersion and the effectiveness of mechanical load transfer depend critically on the interfacial bonding between the nanofiller and the cement matrix. We propose a strong "ionic bridging" mechanism that anchors the polymer-coated nanotubes to the cement hydrates. The cement pore solution is highly alkaline (pH > 12) and becomes saturated with divalent calcium cations (Ca^{2+}) due to the hydration of tricalcium silicate (C_3S) and dicalcium silicate (C_2S), which generate calcium silicate hydrate (C–S–H) gel contributing to strength development, along with calcium hydroxide ($Ca(OH)_2$) [66]. The PEDOT:PSS coating on the MWNT features an outer shell rich in negatively charged sulfonate groups (SO^{3-}) from the PSS chains. A strong electrostatic attraction forms between the Ca^{2+} ions in the pore solution and the anionic SO^{3-} groups on the nanotube surface. This creates robust ionic bonds that firmly anchor the nanofillers to the growing C-S-H gel matrix. This interaction is significantly stronger than the weak van der Waals forces that govern the interface of bare CNT, explaining both the excellent mechanical load transfer observed and the long-term stability of the conductive network. XPS spectra (Fig. S6) elucidate the interfacial chemistry between PEDOT:PSS and cement hydration products. The C 1 s spectrum shows dominant sp^2-hybridized carbons at 284.5 eV and a C-S contribution at 285.7 eV, confirming the integrity of PSS sulfonic acid groups, while the 289.5 eV peak corresponds to carbonate ($CaCO_3$). The O 1 s spectrum (531.7 eV) is consistent with C-O environments from both PEDOT:PSS and cement hydrates. The Ca $2p_{3/2}$ peak at 347.3 eV and the S 2p peaks at 168.8 eV are particularly significant: their coexistence indicates the formation of Ca–SO_3 coordination bonds. This direct spectroscopic evidence strongly supports the proposed ionic bridging mechanism, wherein Ca^{2+} ions from C-S-H gel

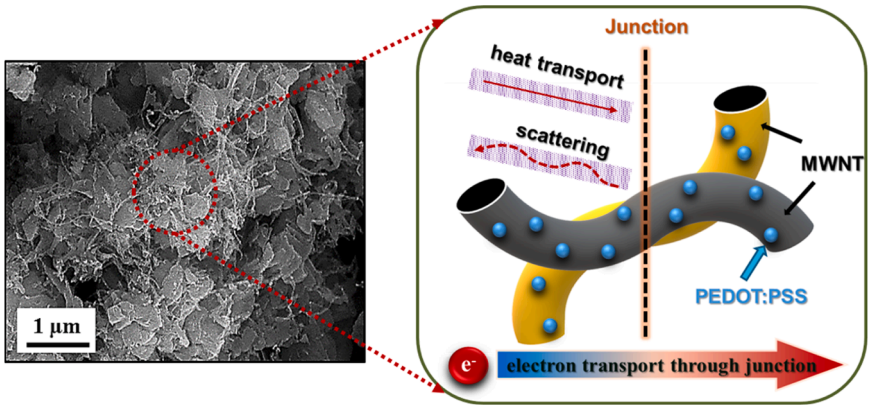

Fig. 7. Schematic illustration of the selective transport mechanism in the hybrid network. The PEDOT:PSS coating on the MWNT forms conductive junctions that enable efficient electron transport, while phonons are effectively scattered at the multiple heterogeneous interfaces (cement-polymer-nanotube), resulting in low *k*. Although this figure is presented as a conceptual schematic, the proposed mechanism is supported by the experimental observations in this study, including enhanced σ (Fig. 3(a)), reduced *k* (Fig. 4), and the SEM-confirmed formation of conductive junctions (Fig. 2).

and portlandite interact electrostatically with SO_3^- groups of PSS. Such interfacial bonding provides enhanced anchoring of polymer-coated CNT within the cement matrix, thereby stabilizing the conductive network and improving load transfer. ATR-FTIR transmittance spectra of neat cement exhibited characteristic bands at 1645 cm^{-1}, 1040 cm^{-1}, and 677 cm^{-1}, consistent with hydrated C-S-H phases (Fig. S7). In the MWNT/PEDOT:PSS–cement composite, new sulfonate bands (~1120 and 1180–1200 cm^{-1}) and a shoulder at ~930–970 cm^{-1} confirm the presence of PSS and PEDOT vibrations. The broadening and slight shifts of these SO_3^- bands, corroborated by XPS, further provide strong evidence of Ca^{2+}–SO_3^- ionic bridging at the polymer-cement interfaces. The combination of a simple, scalable, aqueous-based fabrication process with superior and balanced properties positions this material system as a significant advancement in the field of TE construction materials. The combination of MWNT and PEDOT:PSS in the cementitious composite produces enhancements that cannot be attributed to either component alone. To elucidate the individual contributions of PEDOT:PSS and MWNT, control experiments were conducted with each component separately incorporated into the cement matrix (Table S1). PEDOT:PSS alone provided negligible improvements in both TE performance and compressive strength, indicating that its function is limited to serving as a dispersant. MWNT alone also failed to enhance TE properties to any meaningful degree, as poor dispersion restricted electrical pathways. However, compressive strength showed a slight increase relative to both the control and the PEDOT:PSS-only system, with a maximum improvement of ~5.6 % at 0.5 wt%. Importantly, when PEDOT:PSS and MWNT were combined, a marked synergistic effect was observed, yielding significant improvements in σ, *S*, and *PF*, as well as the highest compressive strength (~19.5 % over plain cement). These findings confirm that the synergy between the two components is essential for realizing simultaneous enhancements in TE and mechanical performance. To further validate the synergistic effect between PEDOT:PSS and MWNT, additional SEM analyses were performed for PEDOT:PSS-cement and MWNT-only cement composites (Fig. S8). The PEDOT:PSS-cement sample showed no distinctive microstructural modification, whereas the MWNT-only cement exhibited agglomerated bundles without interfacial integration. In contrast, the hybrid PEDOT:PSS/MWNT system achieved uniform dispersion and strong ionic bridging with hydration products, confirming that the synergy originates from the pre-stabilization of MWNTs in the PEDOT:PSS matrix prior to cement incorporation.

PEDOT:PSS acts as both a conductive polymeric phase and a dispersing medium, enabling a homogeneous distribution of MWNT within the matrix. This dual role minimizes agglomeration and promotes the formation of a continuous, hybrid conductive network at lower MWNT loadings. In terms of TE behavior, this network facilitates efficient charge carrier transport while maintaining a balanced *S* by reducing junction resistance and controlling carrier scattering. Mechanically, the polymer phase improves interfacial compatibility between the carbon nanotubes and the inorganic matrix, which enhances stress transfer and results in higher compressive strength. Thermally, MWNT contribute high-conductivity channels for phonon transport, while the PEDOT:PSS coating introduces scattering sites that limit excessive thermal conduction, helping to preserve ZT performance. This synergy, stemming from complementary electrical, mechanical, and thermal functionalities, demonstrates the integrated performance benefits achievable through carefully engineered hybrid networks.

4. Conclusion

In this study, we have successfully developed and characterized a novel class of high-performance TE cement composites by leveraging a PEDOT:PSS-assisted dispersion of MWNT. This work addresses the critical, long-standing challenge of nanofiller agglomeration in cementitious systems and demonstrates a scalable, aqueous-based approach to creating multifunctional structural materials. The conductive polymer PEDOT:PSS was shown to be a highly effective additive, serving a dual function as both a polymeric dispersant that ensures homogeneous distribution of MWNT and as an active p-type component contributing to the material's thermoelectric properties. The composite properties were found to be highly dependent on the MWNT concentration. The optimal composition for mechanical performance was 0.5 wt% MWNT, which yielded a compressive strength of 33.1 MPa, a 19.5 % improvement over the plain cement matrix. The peak thermoelectric power factor of 1.33×10^{-5} $\mu W/m \bullet K^2$ was achieved at a lower concentration of 0.5 wt% MWNT. We have proposed and provided evidence for the core mechanisms governing the material's enhanced performance. These include a "double percolation" model for robust charge transport, strong ionic interfacial bonding between the PSS-coated nanotubes and the calcium-rich cement matrix for effective load transfer, and hypothesized enhanced phonon scattering at the complex organic-inorganic interfaces, which likely results in low thermal conductivity. This research establishes a robust and promising pathway toward the practical realization of smart infrastructure, where building components can simultaneously provide structural support and harvest waste thermal energy from their environment. Future research will focus on enhancing the intrinsic conductivity of PEDOT:PSS through post-treatment strategies such as polar solvent or acid treatments, and on evaluating the temperature-dependent thermoelectric behavior and long-term environmental stability of cement composites under conditions including

humidity and freeze–thaw cycles. These studies will provide deeper insights into optimizing performance and validating the practical applicability of PEDOT:PSS/MWNT-cement composites.

CRediT authorship contribution statement

CHO CHUNGYEON: Writing – review & editing, Writing – original draft, Project administration, Methodology, Investigation, Conceptualization. **Sejin Choi:** Writing – original draft, Project administration, Investigation. **Jung Sang Cho:** Methodology, Investigation, Data curation. **Kyungwho Choi:** Methodology, Investigation. **Inyoung Lee:** Methodology, Investigation, Data curation. **Lim Seok Hoon:** Methodology, Investigation, Data curation, Conceptualization. **Jae In Lee:** Investigation, Data curation, Conceptualization.

Declaration of Competing Interest

The authors declare that they have no known competing financial interests or personal relationships that could have appeared to influence the work reported in this paper.

Acknowledgements

This work was supported by the National Research Foundation of Korea (NRF) grant funded by the Korea government (MSIT) (No. RS-024-00405537). This research was also supported by the Institute of Information and Communications Technology Planning and Evaluation (IITP)-Innovative Human Resource Development for Local Intellectualization program grant funded by the Korea government (MSIT) (IITP-2025-RS-2024–00439292).

Appendix A. Supporting information

Supplementary data associated with this article can be found in the online version at doi:10.1016/j.conbuildmat.2025.144440.

Data availability

Data will be made available on request.

References

[1] S. Franco, V.R. Mandla, K.R.M. Rao, Urbanization, energy consumption and emissions in the Indian context A review, Renew. Sust. Energ. 71 (2017) 898–907.
[2] R. Freer, A.V. Powell, Realising the potential of thermoelectric technology: a Roadmap, J. Mater. Chem. C. 8 (2020) 441–463.
[3] X.L. Shi, L. Wang, W. Lyu, T. Cao, W. Chen, B. Hu, Z.G. Chen, Advancing flexible thermoelectrics for integrated electronics, Chem. Soc. Rev. 53 (2024) 9254–9305.
[4] H. Alghamdi, C. Maduabuchi, K. Okoli, M. Alobaid, M. Alghassab, A.S. Alsafran, M. Alkhedher, Latest advancements in solar photovoltaic-thermoelectric conversion technologies: thermal energy storage using phase change materials, machine learning, and 4E analyses, Int. J. Energy Res. 1 (2024) 1050785.
[5] G. Tan, L.D. Zhao, M.G. Kanatzidis, Rationally designing high-performance bulk thermoelectric materials, Chem. Rev. 116 (2016) 12123–12149.
[6] Z. Tian, S. Lee, G. Chen, Heat transfer in thermoelectric materials and devices, J. Heat. Transf. 135 (2013) 061605.
[7] J. Wei, L. Yang, Z. Ma, P. Song, M. Zhang, J. Ma, X. Wang, Review of current high-ZT thermoelectric materials, J. Mater. Sci. 55 (2020) 12642–12704.
[8] M. Channegowda, R. Mulla, Y. Nagaraj, S. Lokesh, S. Nayak, S. Mudhulu, A. Khosla, Comprehensive insights into synthesis, structural features, and thermoelectric properties of high-performance inorganic chalcogenide nanomaterials for conversion of waste heat to electricity, ACS Appl. Energy Mater. 5 (2022) 7913–7943.
[9] F. Kim, B. Kwon, Y. Eom, J.E. Lee, S. Park, S. Jo, J.S. Son, 3D printing of shape-conformable thermoelectric materials using all-inorganic Bi2Te3-based inks, Nat. Energy 3 (2018) 301–309.
[10] O. Caballero-Calero, J.R. Ares, M. Martín-González, Environmentally friendly thermoelectric materials: high performance from inorganic components with low toxicity and abundance in the earth, Adv. Sustain. Syst. 5 (2021) 2100095.
[11] A. Bahrami, G. Schierning, K. Nielsch, Waste recycling in thermoelectric materials, Adv. Energy Mater. 10 (2020) 1904159.
[12] Q. Zhang, Y. Sun, W. Xu, D. Zhu, Organic thermoelectric materials: emerging green energy materials converting heat to electricity directly and efficiently, Adv. Mater. 26 (2014) 6829–6851.
[13] J.L. Blackburn, A.J. Ferguson, C. Cho, J.C. Grunlan, Carbon-nanotube-based thermoelectric materials and devices, Adv. Mater. 30 (2018) 1704386.
[14] H. Wang, C. Yu, Organic thermoelectrics: materials preparation, performance optimization, and device integration, Joule 3 (2019) 53–80.
[15] C. Cho, K.L. Wallace, P. Tzeng, J.H. Hsu, C. Yu, J.C. Grunlan, Outstanding low temperature thermoelectric power factor from completely organic thin films enabled by multidimensional conjugated nanomaterials, Adv. Energy Mater. 6 (2016) 1502168.
[16] C. Cho, Y. Song, J.H. Hsu, C. Yu, D.L. Stevens, J.C. Grunlan, Organic thermoelectric thin films with large p-type and n-type power factor, J. Mater. Sci. 56 (2021) 4291–4304.
[17] X. Fan, W. Nie, H. Tsai, N. Wang, H. Huang, Y. Cheng, Y. Xia, PEDOT: PSS for flexible and stretchable electronics: modifications, strategies, and applications, Adv. Sci. 6 (2019) 1900813.
[18] J. Yang, H.L. Yip, A.K.Y. Jen, Rational design of advanced thermoelectric materials, Adv. Energy Mater. 3 (2013) 549–565.
[19] S. Liu, H. Li, C. He, Simultaneous enhancement of electrical conductivity and seebeck coefficient in organic thermoelectric SWNT/PEDOT: PSS nanocomposites, Carbon 149 (2019) 25–32.
[20] C. Xu, S. Yang, P. Li, H. Wang, H. Li, Z. Liu, Wet-spun PEDOT, PSS/CNT composite fibers for wearable thermoelectric energy harvesting, Compos. Commun. 32 (2022) 101179.
[21] S.H. Chung, D.H. Kim, H. Kim, H. Kim, S.W. Jeong, Thermoelectric properties of PEDOT: PSS and acid-treated SWCNT composite films, Mater. Today Commun. 23 (2020) 100867.
[22] Yunxiao Zhang, Y. Ou, L. Wu, A. Fu, Y. Weng, D. Mao, Exploring the interlaminar toughening potential of carbon nanoparticles: Structural and size effects, Compos. Commun. 47 (2024) 101859.
[23] N. Wen, X. Guan, X. Zuo, Y. Guo, Z. Chen, C. Li, H. Xu, L. Pan, Z. Fan, Investigations of morphology and carrier transport characteristics in high-performance PEDOT: PSS/tellurium binary composite fibers produced via continuous wet-spinning, Adv. Funct. Mater. 34 (2024), 2315677.
[24] J. Milad, M. Saeed, S. Fahimehsadat, P.W. Roger, P. Amir, Thermoelectric energy conversion in buildings, Mater. Today Energ. 32 (2023) 101257.
[25] M. Davoodabadi, I. Vareli, M. Liebscher, L. Tzounis, M. Sgarzi, A.S. Paipetis, V. Mechtcherine, Thermoelectric energy harvesting from single-walled carbon nanotube alkali-activated nanocomposites produced from industrial waste materials, Nanomater 11 (2021) 1095.
[26] J. Wei, Z. Jia, Y. Wang, Y. Jiang, Z. Miao, Y. Zhou, H. Zhang, Enhanced thermoelectric performance of low carbon cement-based composites by reduced graphene oxide, Energy Build. 250 (2021) 111279.
[27] Y. Sargam, K. Wang, J.E. Alleman, Effects of modern concrete materials on thermal conductivity, J. Mater. Civ. Eng. 32 (2020) 04020058.
[28] S. Al Martini, A. Khartabil, R. Sabouni, Evaluation of thermal conductivity of sustainable concrete having supplementary cementitious materials (SCMs) and recycled aggregate (RCA) using needle probe test, Sustain 15 (2022) 109.
[29] R. Piao, G.W. Kim, B. Chun, T. Oh, J.W. Jeong, D.Y. Yoo, Achieving thermoelectric properties of ultra-high-performance concrete using carbon nanotubes and fibers, Renew. Sust. Energ. 199 (2024) 114496.
[30] V.P. Singh, M. Kumar, R.S. Srivastava, R. Vaish, Thermoelectric energy harvesting using cement-based composites: a review, Mater 21 (2021) 100714.
[31] L. Tzounis, M. Liebscher, R. Fuge, A. Leonhardt, V. Mechtcherine, P-and n-type thermoelectric cement composites with CVD grown p-and n-doped carbon nanotubes: demonstration of a structural thermoelectric generator, Energy Build. 191 (2019) 151–163.
[32] X. Zhang, W. Lu, G. Zhou, Q. Li, Understanding the mechanical and conductive properties of carbon nanotube fibers for smart electronics, Adv. Mater. 32 (2020) 1902028.
[33] Y. Wu, X. Zhao, Y. Shang, S. Chang1, L. Dai, A. Cao, Application-driven carbon nanotube functional materials, ACS Nano 15 (2021) 7946–7974.
[34] Lazaros Tzounis, M. Liebscher, R. Fuge, A. Leonhardt, V. Mechtcherine, P- and n-type thermoelectric cement composites with CVD grown p- and n-doped carbon nanotubes: demonstration of a structural thermoelectric generator, Energy Build. 191 (2019) 151–163.
[35] J. Wei, Y. Fan, L. Zhao, F. Xue, L. Hao, Q. Zhang, Thermoelectric properties of carbon nanotube reinforced cement-based composites fabricated by compression shear, Ceram. Int. 44 (2018) 5829–5833.
[36] Q. Zhang, L. Wang, M. Gao, S. Zhao, Surfactants effects on the self-healing properties of asphalt mixtures in a water environment, CSCM 19 (2023) e02585.
[37] Y.Y. Huang, E.M. Terentjev, Dispersion of carbon nanotubes: mixing, sonication, stabilization, and composite properties, Polymers 4 (2012) 275–295.
[38] B.I. Kharisov, O.V. Kharissova, A.V. Dimas, The dispersion, solubilization and stabilization in “solution” of single-walled carbon nanotubes, RSC Adv. 6 (2016) 68760–68787.
[39] X. Zhang, B.W. Li, L. Dong, H. Liu, W. Chen, Y. Shen, C.W. Nan, Superior energy storage performances of polymer nanocomposites via modification of filler/polymer interfaces, Adv. Mater. Interfaces 5 (2018), 1800096.
[40] R. Salehiyan, S.S. Ray, Tuning the conductivity of nanocomposites through nanoparticle migration and interface crossing in immiscible polymer blends: A review on fundamental understanding, Macromol. Mater. Eng. 304 (2019) 1800431.
[41] Y. Gao, F. Zou, H. Sui, J. Xu, S. Wang, S. Lu, J. Yu, Y. Liu, J. Chen, L. Zhao, Dispersion strategies development for high-performance carbon nanomaterials-

reinforced cementitious composites – critical review on properties and future challenges, Mater. Des. 259 (2025) 114789.
[42] Y. Gao, H. Jing, Z. Zhao, X. Shi, L. Li, Influence of ultrasonication energy on reinforcing-roles of CNTs to strengthen ITZ and corresponding anti-permeability properties of concrete, Constr. Build. Mater. 303 (2021) 124451.
[43] W. Chen, Y. Liu, J. Wu, S. Lu, G. Han, X. Wei, Y. Gao, Enhancing cementitious grouting performance through carbon nanotube-coated fly ash incorporation, Constr. Build. Mater. 409 (2023) 133907.
[44] F.Y. Al-Saffar, L.S. Wong, S.C. Paul, An elucidative review of the nanomaterial effect on the durability and calcium-silicate-hydrate (CSH) gel development of concrete, Gels 9 (2023) 613.
[45] A.B. Sabet, S.A.H. Hashemi, R. Farokhzad, A. Delnavaz, Synergic effect of defects on carbon nanoparticles under interaction with calcium silicate hydrate composites, Appl. Surf. Sci. 622 (2023) 156712.
[46] Y. Gao, J. Luo, Z. Li, F. Teng, J. Zhang, S. Gao, and1, X. Tao, Dispersion of carbon nanotubes in aqueous cementitious materials: a review, Nanotechnol. Rev. 12 (2023), 20220560.
[47] P. Damlin, M. Suominen, M. Heinonen, C. Kvarnström, Non-covalent modification of graphene sheets in PEDOT composite materials by ionic liquids, Carbon 93 (2015) 533–543.
[48] A.1 Mora, P. Verma, S. Kumar, Electrical conductivity of CNT/polymer composites: 3D printing, measurements and modeling, Compos. B Eng. 183 (2020) 107600.
[49] W. Bauhofer, J.Z. Kovacs, A review and analysis of electrical percolation in carbon nanotube polymer composites, Compos. Sci. Technol. 69 (2009) 1486.
[50] S.H. Kim, R. Piao, S.K. Lee, T.G. Oh, B.K. Chun, J.W. Jeong, H.J. Lee, D.Y. Yoo, Thermoelectric cement-based composites containing carbon nanotubes (CNTs): effects of water-to-cement ratio and CNT dosage, Case Stud. Constr. Mater. 21 (2024) e03861.
[51] M. Bhandari, J. Yue, I.W. Nam, Mechanical, electrical and fractural characteristics of carbon nanomaterial-added cement composites, Appl. Sci. 15 (2025) 9.
[52] S.H. Jung, S.W. Oh, S.W. Kim, J.H. Moon, Effects of CNT dosange in cement composites on the mechanical properties and hydration reaction with low water-to-binder ratio, Appl. Sci. 9 (2019) 21.
[53] J. Wei, Y. Fan, L. Zhao, F. Xue, L. Hao, Q. Zhamg, Thermoelectric properties of carbon nanotube reinforced cement-based composites fabricated by compression shear, Ceram. Int. 44 (2018) 6.
[54] K.W. Choi, D.Y. Kim, W.S. Chung, C. Cho, S.W. Kang, Nanostructed thermoelectric composites for efficient energy harvesting in infrastructure construction applications, Cem. Concr. Compos 128 (2022) 104452.
[55] J. Wei, Y. Wang, X. Li, Z. Jia, S. Qiao, Q. Zhang, J. Du, Effects of porosity and crack on the thermoelectric performance of expanded graphite/carbon fiber reinforced cement-based composites, Int. J. Energy Res. 44 (2020) 6885.
[56] S. Ghosh, B.B. Saha, Estimation energy harvesting by thermoelectric cement composites with nanostructured graphene and metallic oxides, J. Compos. Sci. 7 (2023) 207.
[57] N. Zhang, W. She, F. Du, K. Xu, Experimental study on mechanical and functional properties of reduced graphene oxide/cement composites, Materials 13 (2020) 3015.
[58] J. Huang, Z. Wang, G. Li, J. Yu, Synergistic effects of carbon nanotubes and polyvinyl alcohol on enhancing mechanical strength and carbonation resistance of concrete, Constr. Build. Mater. 492 (2025) 143036.
[59] H.A. Umar, X. Zeng, X. Hu, M.J. Garba, G. Long, C. Shi, Impact response of self-compacting concrete incorporating asphalt emulsion and fiber, Constr. Build. Mater. 474 (2025) 141056.
[60] S.-H. Hong, J.-S. Choi, S.-J. Yoo, D.-Y. Yoo, Y.-S. Yoon, Reinforcing effect of CNT on the microstructure and creep properties of high-strength lightweight concrete, Constr. Build. Mater. 428 (2024) 136294.
[61] P. Stynoski, P. Mondal, C. Marsh, Effects of silica additives on fracture properties of carbon nanotube and carbon fiber reinforced Portland cement mortar, Cem. Concr. Compos 55 (2015) 232–240.
[62] Y. Song, J. Tang, Y. Qi, J. Zhang, Y. Li, F. Wang, A review on the dominating factor for the conductivity enhancement of PEDOTs: the affinity of polyanion shell toward post-processing reagents? Polymer 266 (2023) 125649.
[63] S. Wei, Y. Zhang, H. Lv, L. Deng, G. Chen, SWCNT network evolution of PEDOT: PSS/SWCNT composites for thermoelectric application, J. Chem. Eng. 428 (2022) 131137.
[64] A.N. Volkov, L.V. Zhigilei, Heat conduction in carbon nanotube materials: strong effect of intrinsic thermal conductivity of carbon nanotubes, Appl. Phys. Lett. 101 (2012) 043113.
[65] K. Bui, B.P. Grady, D.V. Papavassiliou, Heat transfer in high volume fraction CNT nanocomposites: effects of inter-nanotube thermal resistance, Chem. Phys. Lett. 508 (2011) 248–251.
[66] X. Wang, K. Xu, Y. Li, S. Guo, Dissolution and leaching mechanisms of calcium ions in cement based materials, Constr. Build. Mater. 180 (2018) 103–108.